A Computational Approach to Magnetic Force Feedback Design

Masa Ogata
National Institute of Advanced Industrial Science and Technology (AIST)
Japan

Yuki Koyama
National Institute of Advanced Industrial Science and Technology (AIST)
Japan

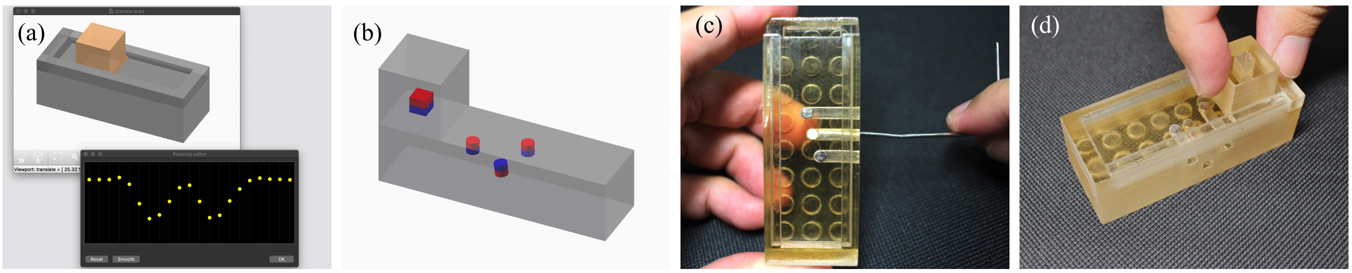

Figure 1: Computational design of magnetic force feedback in digital fabrication. (a) The user specifies the target 3D model (consisting of a movable part and a fixed part) and the desired haptic force feedback. (b) Our method computationally solves an inverse problem to obtain an optimal arrangement of magnets that renders the desired force feedback. (c) The user can easily fabricate the model and embed magnets into the holes. (d) The user obtains the desired haptic force feedback during interacting with the fabricated object.

ABSTRACT

We present a computational approach to haptic design embedded in everyday tangible interaction with digital fabrication. To generate haptic feedback, the use of permanent magnets as the mechanism potentially contributes to simpleness and robustness; however, it is difficult to manually design how magnets should be embedded in the objects. Our approach enables the inverse design of magnetic force feedback; that is, we computationally solve an inverse problem to obtain an optimal arrangement of permanent magnets that renders the user-specified haptic sensation. To solve the inverse problem in a practical manner, we also present techniques on magnetic simulation and optimization. We demonstrate applications to explore the design possibility of augmenting digital fabrication for everyday use.

CCS CONCEPTS

• **Human-centered computing → Human computer interaction (HCI)**.

KEYWORDS

Haptics, Magnetic force feedback, Inverse design, Optimization, Digital fabrication

ACM Reference Format:

Masa Ogata and Yuki Koyama. 2021. A Computational Approach to Magnetic Force Feedback Design. In *CHI Conference on Human Factors in Computing Systems (CHI '21), May 8–13, 2021, Yokohama, Japan.* ACM, New York, NY, USA, 11 pages. https://doi.org/10.1145/3411764.3445631

1 INTRODUCTION

Haptic design is essential for humans to understand the functionality of tools. In tangible interaction, producing appropriate haptics can enhance usability and a sense of immersion. Actuators can contribute to haptic design with interactivity; however, the scope is limited considering the implementation constraint. Aiming design for everyday use, we focus on a physical mechanism for haptic design. Some of the mechanical components are designed as a haptic device, but its design is generally normalized in industry and not flexible. The magnetic force can be a mechanism for rendering haptics and has a significant advantage with digital fabrication since it is simple, compact, contactless, and non-abrasion. Hence, our motivation is to achieve haptic design using magnetic forces embedded in tangible interaction.

However, designing haptics using magnetic forces is highly challenging. Magnetic force is non-intuitive for the kinesthetic sense of the human body. For example, the attraction force between two magnets changes unexpectedly in close distance. Besides, for our purpose, a magnetic force can be perceived when the user moves the movable component of an everyday object with embedded magnets; in this case, the magnetic force is hugely affected by not only the trajectory of the moving magnet but also the orientations of other magnets embedded in the fixed component. With some other difficulties, the user will face problems when deciding the spatial relationship of all magnets because the manual design of magnets' position and orientation in three-dimensional models is a highly complicated task.

In this paper, we propose a computational approach to magnetic force feedback design. As shown in Figure 1, the user effortlessly

CHI '21, May 8–13, 2021, Yokohama, Japan

builds a mechanical component for tangible interaction by specifying the desired curve of the force feedback by drawing. Even with the support of the forward simulation [18], it was difficult for the user to design by manual. To achieve our goal, we formulate this inverse design problem from the perspective of numerical optimization and propose an optimization method with several non-trivial techniques. We demonstrate the effectiveness of this approach by creating various objects with desired haptics using digital fabrication.

2 RELATED WORKS

2.1 Haptic Design by Magnetic Force

Magnetic force has not been widely discussed as a potential source of haptic feedback. To the best of our knowledge, Hayward [9] firstly reported the relationship between haptics and magnetic force, with mentioning similarity to lateral force fields reported in [26]. As the capability of magnetic force, haptic design with a magnetic force is a popular method in human-computer interaction (HCI). Designing tactile feedback using a rubber magnet with a magnetization pattern is done by [35, 36]. Mechamagnets [39] performed design exploration of a haptic mechanism with permanent magnets. Magneto-haptics [18] also explored forward simulation for designing magnetic force with permanent magnets. However, a relationship between magnetic force and haptics has not been discussed in previous works. In this paper, we formally discuss this relationship to solve the inverse design to achieve the automatic design of the magnetic force.

Active haptic devices, such as actuator and vibrator, had been used for haptics with computation from an early stage [14]. We here mention some examples using the active haptic device with a magnetic force. MaglevHaptics [10] performed a haptic device designed with magnetic levitation. FingerFlux [34] is a technical approach to generate haptic sensation via magnetic flux from an array of the electromagnet. FluxPaper [19] tried vibration via magnetized paper using array of electromagnets. Omni [13] is a haptic feedback system in which sensing and actuation are enabled by detecting the 3D position of a magnet embedded in a passive tool.

2.2 Simulation in Electromagnetism

There are mainly two approaches to simulate electromagnetism; analytical and numerical. For solving the magnetic force between two magnets, some analytical calculations were proposed in the early stage. As a numerical solution, the finite element method (FEM) is the most famous for solving many problems in physics. However, the computation cost of FEM in three-dimensional space is very high. An approximate analytical approach to calculate magnetic forces between two magnets was developed using Taylor expansion [37]. This approach was also utilized in the computer graphics community [30]. Magneto-Haptics [18] also utilized this approach for forward simulation of magnetic force to estimate haptic feedback for designing tangible interaction. We follow them and use this approximate approach. Note that some advanced magnetic simulation methods tailored for specialized scenarios [11, 16] have been proposed recently, but these features are not necessary for our target scenarios. Also note that the concepts from magnetostatics used in this paper are explained in details in [5].

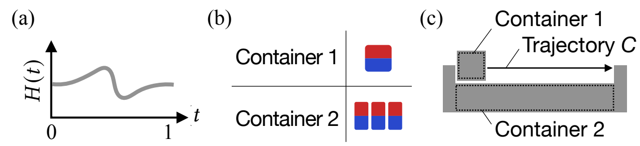

Figure 2: Input from the user. It consists of (a) the desired curve of haptic sensation, (b) the geometry and maximum number of magnets, and (c) the containers and trajectory.

2.3 Computational Inverse Design

Computational design methods aim at finding optimal design parameters that maximize desired properties by computationally solving optimization problems. Researchers have taken this approach in various domains [3, 12, 20, 25, 32]; for example, the target property could be the balancing capability of 3D printed objects [3, 25] or the user performance in graphical user interface [20]. Inverse design is considered as a variant of computational design, where the user directly specifies the property that the final outcome should have, and the optimization solver tries to reproduce the property. This approach is useful for fabrication scenarios, and researchers have investigated inverse design methods that reproduce user-specified mechanical properties [27, 38], deformations [4, 29], colors [2, 6], and shapes [8, 15] of fabricated objects. Our work investigates an inverse design approach to reproduce the user-specified haptics using embedded permanent magnets.

Several researchers have investigated the inverse design of haptics in different scenarios. Fujinawa et al. [7] proposed a method of designing hand-held objects that provide illusional haptic shape perception. Piovarci et al. [24] proposed a method of optimizing 3D printing materials to design perceptual elasticity in touch interaction. Researchers have also investigated methods of achieving the inverse design of tactile textural feedback for fingertips [31] and styli for drawing [22, 23]. Our work is the first to investigate the inverse design of magnetic force feedback, which enables end-users to design new interactions with everyday objects, and we propose several techniques to achieve this concept.

3 INTERACTION OVERVIEW

We propose a computational approach to design magnetic force feedback in three-dimensional models for digital fabrication. A spatial arrangement of magnets that fulfills the desired magnetic force feedback can be automatically explored and optimized in software. The user specifies the desired curve of force feedback by drawing and then obtains a functional three-dimensional model with spaces hollowed out for permanent magnets. The software only requires some instruction about the movable component, without asking any knowledge of magnetism.

3.1 Input and Output

The user needs to specify the followings as input (see Figure 2).

- The desired curve of haptic sensation (annotated as $H(t)$).
- The geometry of containers.
- The trajectory that one of the containers moves with.
- The geometry of magnet for each container.

Table 1: Geometry of the magnets used in the applications. Sizes represent Width-Depth-Height for cubes, and Diameter-Height for cylinders (in millimeters). All magnets are magnetized in the height direction.

	Container 1		Container 2	
	Type	Size	Type	Size
Slider (1)	Cube	$4 \times 3 \times 6$	Cylinder	3×6
Slider (2)	Cube	$5 \times 5 \times 2$	Cube	$5 \times 5 \times 2$
Slider (3)	Cube	$4 \times 4 \times 4$	Cylinder	3×3
Dial (1)	Cylinder	4×4	Cylinder	4×4
Dial (2)	Cylinder	4×3	Cylinder	3×4
Case (1)	Cube	$3 \times 24 \times 2$	Cylinder	3×6

- The maximum number of magnets.

The software then outputs an optimal arrangement of magnets, i.e., how we should embed magnets into the containers. In this work, the number of containers is assumed to be two for simplicity. As for the magnet material, the Neodymium magnet (N35 grade, which is very popular in the market) is used by default. The user can change the magnetic material by setting the value of residual magnetism.

3.2 Example Applications

Figure 3 outlines example applications of physical interface components that demonstrate haptic design by magnetic force. Three types of components are demonstrated: slider, dial, and case. The user prepared the 3D models, and the system automatically hollowed holes for embedding magnets after fabrication by 3D printing. The used magnets are summarized in Table 1. These geometries were empirically chosen for each applications after several trials with considering the solution quality.

Slider. This component has a small movable block that moves on the linear trajectory. Inputting different kinds of target curves, we obtained three unique arrangements. Slider (1) only uses three magnets to achieve a single cycle of a sawtooth wave. Slider (2) performs a non-trivial arrangement to achieve linear force feedback only using three magnets; besides the magnetic force between two magnets is known as non-linear to the distance. Slider (3) shows that the system managed sharp spots by arranging magnets effectively.

Dial. This component has a movable disk-shape part that moves on a rotational trajectory. The rotation angle is limited to 180 degrees on the system. For Dial (1), we tried to find the optimal arrangements which achieve bump and hole illusion. Dial (2) performs a small spot to give a stable position of haptic sensation.

Case. This component has single rid moves on a rotational trajectory with two holes. Usually, the magnetic force implemented for those case design is too abrupt for the user when closing. We tried to create linear force feedback to ease the magnetic force when closing the rid. In order to reduce the number of magnets, the flat and long magnet for container 1 was selected. The rotation angle is limited to 45° on the system.

3.3 Difficulty of Problem

The need for inverse design comes from the difficulties in manual design. There are mainly two reasons. (1) Small changes in the orientation of any magnet drastically affect the magnetic force. This is because the magnetic force in the magnetic field is position-dependent, and the superposed magnetic field leaked from multiple magnets is highly complicated. (2) The space of parameters to explore is highly broad and indirect. The magnetic force applied to the movable magnet is varying on the trajectory, which requires careful consideration of how multiple magnets affect the time-varying magnetic force in combination.

4 TECHNICAL OVERVIEW

We formulate the haptics design problem as an inverse optimization problem. That is, given a desired *haptic potential field* (described as haptic sensation in Section 3) specified by the user, we want to find an optimal arrangement of magnets that reproduces the desired haptic potential field as closely as possible. The magnetic simulation is iteratively performed in our optimization process. Figure 4 shows the overview of the process.

Notations. We denote by $H \in \mathcal{H}$ a haptic potential field (which can be represented as a curve), where $\mathcal{H}$ is the set of all the possible haptic potential fields. We especially denote by $H^{\text{target}} \in \mathcal{H}$ the target haptic potential field that is specified by the user. We denote by $\mathbf{x} \in \mathcal{X}$ an arrangement of magnets, where $\mathcal{X}$ is the set of all the possible magnet arrangements. Note that the number of magnets is not a constant in our problem setting (i.e., it can be an arbitrary number that is more than or equal to two), and thus we use $\mathbf{x}$ as a *trans-dimensional* variable; for example, $\mathbf{x}$ may implicitly represent a spatial arrangement of two magnets, or that of five magnets. We write $H(\mathbf{x}) \in \mathcal{H}$ for the simulated haptic potential field that the magnet arrangement $\mathbf{x}$ generates. Finally, we denote by $\mathbf{x}^* \in \mathcal{X}$ the optimal magnet arrangement that we want to obtain by solving the optimization problem.

Mathematical Formulation. This inverse design problem can be mathematically described as an optimization problem:

$$\mathbf{x}^* = \mathop{\arg\min}_{\mathbf{x} \in \mathcal{X}} d(H(\mathbf{x}), H^{\text{target}}) \quad \text{subject to} \begin{cases} \text{all magnets are inside the container} \\ \text{all magnets are collision-free} \end{cases}, \tag{1}$$

where $d : \mathcal{H} \times \mathcal{H} \to \mathbb{R}_{\geq 0}$[1] is a distance function that quantifies how much the two haptic potential fields differ (formally defined in Section 7.2). For example, $d(H_1, H_2)$ returns zero when H_1 and H_2 are exactly the same, and it returns a positive value when H_1 is different from H_2. The solution $\mathbf{x}^*$ is the magnet arrangement that minimizes the distance between the simulated haptic potential field and the target haptic potential field, while it satisfies the two constraints, "all magnets are inside the container" and "all magnets are collision-free."

Technical Challenges. This optimization problem is highly challenging to solve; it is considered as a constrained non-linear global optimization, and the number of its dimensions is not fixed since

[1] Here $\mathbb{R}_{\geq 0}$ denotes the set of real numbers that are greater than or equal to zero. We will use similar notations in the reminder of the paper.

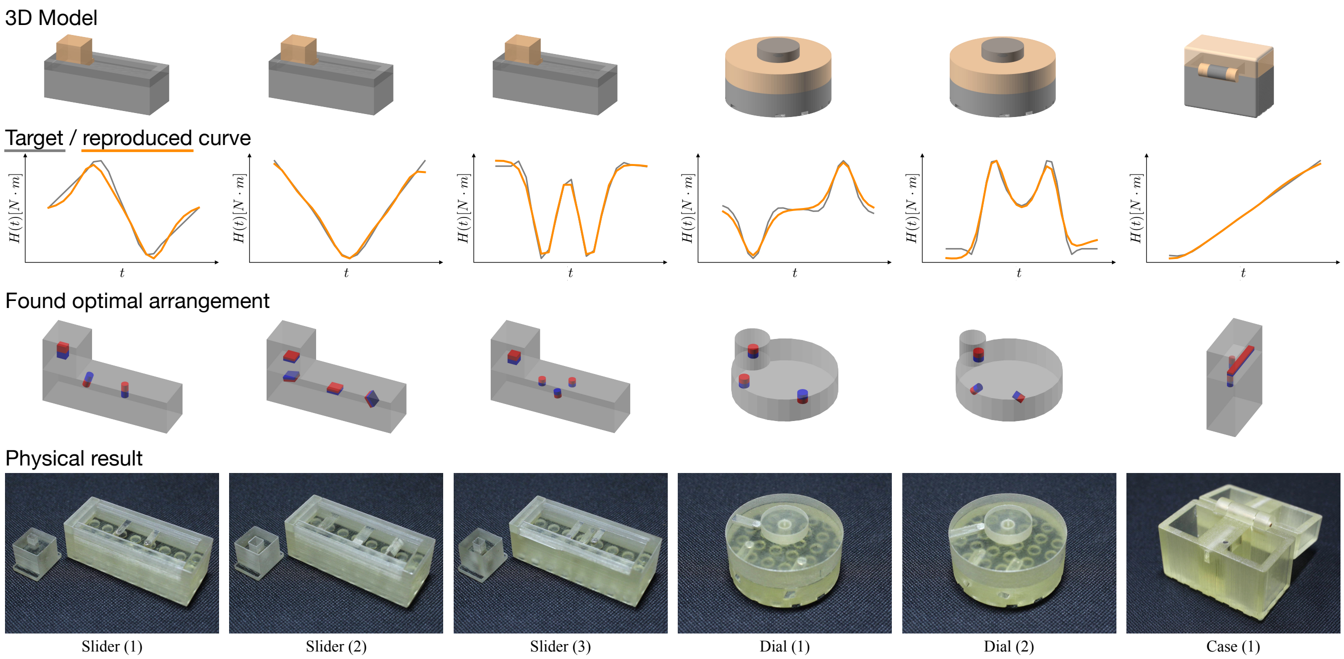

Figure 3: 3D models and result of optimization with actual output fabricated by 3D printer and embeded permanent magnets.

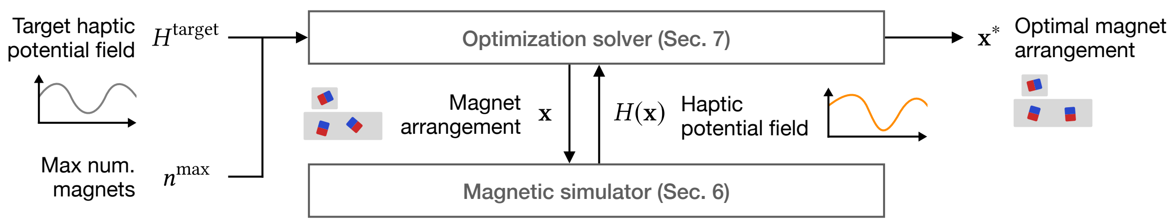

Figure 4: Overview of the inverse design process. The input to the optimization solver consists of the target haptic potential field H^{target} and the maximum number of magnets $n^{\max}$. The optimization solver then performs iterative search, which involves the magnetic simulator in its loop. Finally, the optimization solver outputs the optimal magnet arrangement $\mathbf{x}^*$.

we do not know beforehand how many magnets should be used. We will detail the technical challenges in Section 7.1. These challengings prevent us from directly applying off-the-shelf optimization libraries; they do not accept this problem type, or at best, they will fail to find plausible solutions in practical amount of time. This motivates us to develop techniques to make this problem tractable.

Technical Contributions. In addition to the primary contribution, i.e., the proposition and demonstration of the computational approach to magnetic force feedback design, we also offer the following technical contributions to achieve this approach. In Section 5, we formalize the definition of the haptic potential field and also describe how it can be interpreted from the viewpoint of physics. In Section 6, we describe new techniques to efficiently simulate magnetic forces to calculate the haptic potential field $H(\mathbf{x})$. In Section 7, we describe how the above optimization problem can be approximately solved by making non-trivial modifications to this problem.

5 DEFINITION OF HAPTIC POTENTIAL FIELD

This section defines and discusses the haptic potential field, denoted as H. The concept itself was firstly introduced by Ogata [18]; however, the original paper lacks formal discussions in physics, and it only provides how the concept is implemented and how visually intuitive it is. For example, although it has "potential" in its name, the paper does not discuss how it relates to the concept of potential in physics. We describe the concept more formally and generally from the viewpoint of physics so that haptics researchers who work on magnetism or want to extend the concept beyond magnetism can refer to this section in the future.

As an intuition, we describe the haptic potential field (which will be defined in Equation 8) in relation to the work that the finger does while manipulating the movable container along with the predetermined trajectory (as we will see in Equations 9 and 14). The finger perceives this work as force feedback during the manipulation.

5.1 Assumptions

First, we assume that all motions occur in the *quasi-static* manner. That is, any time derivatives (e.g., velocity and acceleration) in the environment are considered sufficiently small and thus ignorable. This assumption also implies that the magnetic field in the environment is always considered steady, and thus we can use magnetostatics. We also assume that the movable container is sufficiently small, and it is considered a point mass (with a mass $m \in \mathbb{R}_{>0}$). Finally, we assume that the movable container can only move along the specified trajectory C because of the design of containers.

5.2 Trajectory

We parametrize the three-dimensional trajectory C by a parameter $t \in [a, b]$, where a represents the starting endpoint and b represents the ending endpoint. Without loss of generality, we assume $a = 0$ and $b = 1$. Let $\mathbf{r}$ be the function that maps t and the corresponding three-dimensional position on the trajectory C. For example, $\mathbf{r}(0) \in \mathbb{R}^3$ and $\mathbf{r}(1) \in \mathbb{R}^3$ are the positions of the starting and ending endpoints of the trajectory C, respectively. Note that the parameter t does not have a physical interpretation, but we call it "time" just for convenience when no confusion can arise.

5.3 Forces

Let $\mathbf{F}_{\text{total}}(t) \in \mathbb{R}^3$ be the total force that the movable container receives at the time t during the motion along the trajectory C. Similarly, let $\mathbf{F}_{\text{finger}}(t)$, $\mathbf{F}_{\text{magnet}}(t)$, $\mathbf{F}_{\text{gravity}}(t)$, and $\mathbf{F}_{\text{container}}(t)$ be the force applied by the finger, the force applied by the magnetic field, the force applied by the gravity, and that force applied by the other (fixed) container, respectively. Then, the relation,

$$\mathbf{F}_{\text{total}}(t) = \mathbf{F}_{\text{finger}}(t) + \mathbf{F}_{\text{magnet}}(t) + \mathbf{F}_{\text{gravity}}(t) + \mathbf{F}_{\text{container}}(t), \quad (2)$$

holds at any time t. By applying Newton's second law to the movable container, we have $\mathbf{F}_{\text{total}}(t) = m\mathbf{a}(t)$, where $\mathbf{a}(t) \in \mathbb{R}^3$ is the acceleration of the movable container at the time t. By the quasi-static assumption, we have $\mathbf{a}(t) = \mathbf{0}$ at any time t. Therefore,

$$\mathbf{F}_{\text{finger}}(t) = -\mathbf{F}_{\text{magnet}}(t) - \mathbf{F}_{\text{gravity}}(t) - \mathbf{F}_{\text{container}}(t) \quad (3)$$

holds at any time t.

5.4 Work Done by Finger

We now consider the work done by the application of the force to the movable container by the finger. We denote by $W_{\text{finger}}(t) \in \mathbb{R}$ the work done until reaching the position $\mathbf{r}(t)$ from the starting position $\mathbf{r}(0)$. By the definition of work, it is written as

$$W_{\text{finger}}(t) = \int_0^t \mathbf{F}_{\text{finger}}(t') \cdot \mathbf{r}'(t') dt', \quad (4)$$

where $\mathbf{r}'(t) = \frac{\partial}{\partial t}\mathbf{r}(t)$, and the centered dot represents the inner product between vectors.

5.5 Potential of Magnetic Force

The magnetic force, $\mathbf{F}_{\text{magnet}}$, needs a special care. Suppose an ideal case of a uniformly magnetized magnet; it can be treated as a simple magnetic moment. However, as actual magnets have various shapes and magnetic fields created by other magnets are not uniform, magnets cannot be treated as magnetic moments to simulate $\mathbf{F}_{\text{magnet}}$ in a feasible way. Thus, we need to utilize numerical analysis to calculate magnetic fields and the magnetic force.

Nevertheless, the force $\mathbf{F}_{\text{magnet}}$ can be considered a conservative force since it is fully specified by the spatial position of the movable container by the magnetostatics assumption. Thus, though no simple closed form is available, we can still define a potential field $U_{\text{magnet}}(t)$ such that $\mathbf{F}_{\text{magnet}}(t) = -\nabla U_{\text{magnet}}(t)$.

5.6 Haptic Potential Field

Considering Equation 3 and Equation 4, the work $W_{\text{finger}}(t)$ can be virtually decomposed into the component by conservative forces (i.e., $-\mathbf{F}_{\text{magnet}}(t) - \mathbf{F}_{\text{gravity}}(t)$), denoted by $W^{\text{con.}}_{\text{finger}}(t)$, and the component by non-conservative forces (i.e., $-\mathbf{F}_{\text{container}}(t)$), denoted by $W^{\text{non-con.}}_{\text{finger}}(t)$. That is,

$$W_{\text{finger}}(t) = W^{\text{con.}}_{\text{finger}}(t) + W^{\text{non-con.}}_{\text{finger}}(t). \quad (5)$$

Let $W_{\text{magnet}}(t)$ be the work done by the application of the magnetic force $\mathbf{F}_{\text{magnet}}(t)$ to the movable container. Similarly, let $W_{\text{gravity}}(t)$ be the work done by the application of the gravitational force $\mathbf{F}_{\text{gravity}}(t)$ to the movable container. Using these notations, we have

$$W^{\text{con.}}_{\text{finger}}(t) = -W_{\text{magnet}}(t) - W_{\text{gravity}}(t). \quad (6)$$

Since they are the work done by conservative forces, it can be written using their potentials as

$$W^{\text{con.}}_{\text{finger}}(t) = \Delta_{0\to t} U_{\text{magnet}} + \Delta_{0\to t} U_{\text{gravity}}, \quad (7)$$

where $\Delta_{a\to b} U = U(b) - U(a)$. Now, we define the haptic potential field[2] $H : [0, 1] \to \mathbb{R}$ as

$$H(t) = U_{\text{magnet}}(t) + U_{\text{gravity}}(t). \quad (8)$$

Since both components are potential fields, H is also a potential field. Using this definition, Equation 7 is written as

$$W^{\text{con.}}_{\text{finger}}(t) = \Delta_{0\to t} H = H(t) - H(0), \quad (9)$$

where $H(0)$ is an arbitrary constant offset. Thus, the landscape (i.e., the curve) of the haptic potential field can be interpreted as the plot of the work done by the finger against conservative forces (with an offset).

It is noteworthy that the haptic potential field does not involve any path-dependent line integrals in its definition; the landscape of H is thus independent of the parameterization of the trajectory C. This is why we call it a field. In other words, it is beneficial for the definition to be independent of the force applied by the fixed container, $\mathbf{F}_{\text{container}}$, since it is a non-conservative force (unlike the gravity force) and thus prohibits us from modeling the haptic sensation from the viewpoint of the potential field. Also, the force may depend on many factors such as the choice of materials, which requires additional assumptions to define the interaction scenario.

[2]By abuse of notation, we here use H as the function of t (representing the value at a point in the field). As described in Section 4, we also continue to use H as the function of $\mathbf{x}$ (representing the entire field) when no confusion can arise.

5.7 Discussion: The Effect of Gravity

If the trajectory C involves only horizontal motions, then $U_{\text{gravity}}(t)$ is constant at any time t, and thus $\Delta U_{\text{gravity}} = 0$ holds. In such cases, we can just ignore the effect of gravity in terms of the haptic potential field. Even when the trajectory C involves some up-down motions, we can consider $\Delta U_{\text{gravity}} = 0$ if the gravitational force $\mathbf{F}_{\text{gravity}} = m\mathbf{g}$, where $\mathbf{g} \in \mathbb{R}^3$ is the gravitational acceleration, is sufficiently smaller than the magnetic force $\mathbf{F}_{\text{magnet}}$. In the following sections of this paper, we assume that we can ignore the gravitational effect for simplicity.

5.8 Discussion: The Effect of Friction

The force applied by the fixed container, $\mathbf{F}_{\text{container}}(t)$, can be decomposed into the frictional component $\mathbf{F}_{\text{friction}}(t)$, which aligns with the moving direction, and the normal component $\mathbf{F}_{\text{normal}}(t)$, which is orthogonal to the frictional component. That is,

$$\mathbf{F}_{\text{container}}(t) = \mathbf{F}_{\text{friction}}(t) + \mathbf{F}_{\text{normal}}(t). \tag{10}$$

Using this notation, the non-conservative component of the work, $W^{\text{non-con.}}_{\text{finger}}$, can be written as

$$W^{\text{non-con.}}_{\text{finger}}(t) = \int_0^t (-\mathbf{F}_{\text{container}}(t')) \cdot \mathbf{r}'(t')dt' \tag{11}$$

$$= -\int_0^t \left\{\mathbf{F}_{\text{friction}}(t') \cdot \mathbf{r}'(t') + \mathbf{F}_{\text{normal}}(t') \cdot \mathbf{r}'(t')\right\} dt' \tag{12}$$

$$= -\int_0^t \mathbf{F}_{\text{friction}}(t') \cdot \mathbf{r}'(t')dt', \tag{13}$$

since $\mathbf{F}_{\text{normal}}(t') \cdot \mathbf{r}'(t')$ is zero at any time t'.

If the frictional force $\mathbf{F}_{\text{friction}}$ is sufficiently small (e.g., by choosing smooth materials for fabrication), we can consider $W^{\text{non-con.}}_{\text{finger}} = 0$. Thus, we have

$$W_{\text{finger}}(t) = \Delta_{0\to t} H = H(t) - H(0). \tag{14}$$

This relationship provides an additional interpretation on the haptic potential field; the landscape (i.e., the curve) of the haptic potential field can be interpreted as the plot of the work done by the finger (with an offset) in an frictionless environment.

6 MAGNETIC SIMULATION TECHNIQUES

We describe both the numerical analysis method to calculate the magnetic force $\mathbf{F}$ applied to the magnet moved by the finger, and the formulation to calculate the haptic potential field $H(t)$. We utilize the Taylor expansion approach, which approximately calculates the magnetic force between two magnets. This approach was originally proposed in [37] and used for simulation in computer graphics [30].

In the Taylor expansion approach, the mesh resolution contributes to the precision. While reducing the number of meshing blocks contributes to the efficiency of calculation cost, a naïve way would sacrifice the precision. Thus, we also describe some techniques to improve the calculation cost while maintaining precision.

6.1 Magnetic Force by Taylor Expansion

Basic formula of magnetic force applied to a magnetic pole is written as $\mathbf{F} = \nabla(\mathbf{m} \cdot \mathbf{B})$. Here, $\mathbf{B}$ means magnetic flux density, which is

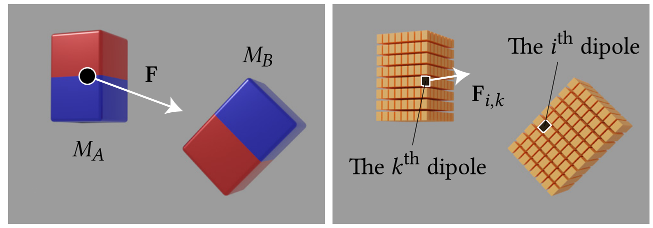

Figure 5: Magnetic force simulation with dipoles. The force F that the magnet M_A receives from the magnet M_B (Left) is considered as the summation of forces between dipoles (Right).

strength of magnetic field though certain surface depending on material. In our purpose, $\mathbf{B}$ is determined as leaked magnetic flux from other magnets. To approximate the magnetic force calculation, we apply Taylor expansion to small sections of the magnet, treating as small magnetic moments (magnetic dipoles) as illustrated in Figure 5. Let $\mathbf{F}$ be the force that the magnet M_A receives from the magnet M_B, and n_A and n_B be the number of grid mesh cells (i.e., dipoles) of M_A and M_B, respectively. Then, the force is calculated as

$$\mathbf{F} = \sum_{k=1}^{n_A} \mathbf{F}_k = \sum_{k=1}^{n_A} \sum_{i=1}^{n_B} \mathbf{F}_{i,k}, \tag{15}$$

where $\mathbf{F}_k$ is the force that the k-th dipole of the magnet M_A receives from the entire magnet M_B, and $\mathbf{F}_{i,k}$ is the force that the k-th dipole of the magnet M_A receives from the i-th dipole of the magnet M_B. Figure 5 illustrates this concept. The force $\mathbf{F}_{i,k}$ is calculated as

$$\mathbf{F}_{i,k} = \frac{\mu_0}{4\pi} \cdot \frac{1}{\|\mathbf{r}_k - \mathbf{r}_i\|^4} \Big[-15\mathbf{n}_{i,k}(\mathbf{m}_k \cdot \mathbf{n}_{i,k})(\mathbf{m}_i \cdot \mathbf{n}_{i,k}) + 3\mathbf{n}(\mathbf{m}_k \cdot \mathbf{m}_i) + 3\big(\mathbf{m}_k(\mathbf{m}_i \cdot \mathbf{n}_{i,k}) + \mathbf{m}_i(\mathbf{m}_k \cdot \mathbf{n}_{i,k})\big)\Big] \tag{16}$$

where $\mathbf{n}_{i,k} = (\mathbf{r}_k - \mathbf{r}_i)/\|\mathbf{r}_k - \mathbf{r}_i\|$, $\mathbf{r}$ is a position of magnetic dipole, and μ_0 is the magnetic constant.

As the magnetic force is superpositional, the magnetic force from multiple magnets can be solved by summarizing each F with each magnet. Still, there is a problem of determining eligible n_A and n_B, which is a split number of the magnet into dipoles. These numbers significantly affect the computation cost. We describe a technique to adaptively determine the split number in the next subsection.

6.2 Haptic Potential Field

As discussed in Section 5.6, we assume $\Delta H = \Delta U$ with ignoring gravitational force. Therefore, the haptic potential field $H(t)$ is treated as equal to the potential field of magnetic force $U(t)$. The potential field $U(t)$ can be obtained from the formula of ΔU:

$$\Delta U = -\int_0^t \mathbf{F}(\mathbf{r}(t')) \cdot \mathbf{r}'(t')dt'. \tag{17}$$

Note that, to extract the component of the magnetic force applied to the direction along the trajectory, the magnetic force must be "normalized" with the direction vector $\mathbf{r}'(t)$ by inner product, as indicated by this equation. By assuming that the trajectory is discretized into some sections, we calculate $\mathbf{F}(\mathbf{r}(t))$, $\mathbf{r}'(t)$, and their

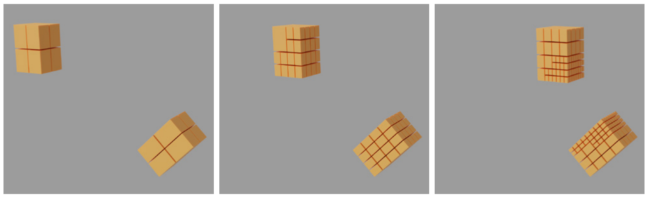

Figure 6: Adaptive meshing. From left to right, the upper magnet comes closer to the bottom magnet. The resolution of the meshes adaptively changes based on the distance, by which the computational cost of the magnetic force simulation can be reduced while the accuracy remains sufficient.

inner product at each section of t. Then, the potential field $U(t)$ can be calculated as a cumulative product[3] of normalized magnetic forces and divided lengths of these sections.

6.3 Adaptive Meshing

When calculating the magnetic force, a pair of closer dipoles affects more than distant ones. To increase the precision of the simulation, it is desirable to execute meshing the closer pair of dipoles finely. However, fine meshing causes high computation costs. Adaptive meshing, i.e., selecting blocks to separate into finer blocks, will help the problem of computation costs. Following the previous work [37], we decided on the condition to apply adaptive meshing. Condition is determined by $\rho \geq 1/7$, where $\rho = d/r$, r is distance between two dipoles, and d is length of dipole. Figure 6 shows time series of adaptive meshing up to depth 4, which is the maximum depth level in our implementation. The number of depth may affect the precision of the magnetic force.

6.4 Interpolation

To reduce computation cost, we also operate interpolation on the magnetic force. We multiplied section four times from the original curve of magnetic force. For example, if the original section of t is 20, it becomes 80, meaning that the computation cost becomes four times smaller. Due to its characteristics, the shape of the magnetic force is always smooth. Therefore, applying the spline interpolation is reasonable, and it does not cause much deviation from the original curve of the magnetic force.

7 OPTIMIZATION TECHNIQUES

7.1 Overview

We want to solve the optimization problem, formulated as Equation 1, in a practical manner. Even with the efficient magnetic force simulation described in Section 6, this problem is still very challenging to solve. This is because the problem has the following properties.

- Trans-dimensional: the number of magnets (and thus the optimization dimensionality) is not fixed beforehand and needs to be determined by the solver.
- Constrained: the optimization variables need to not only minimize the objective but also satisfy the constraints.

[3] https://numpy.org/doc/stable/reference/generated/numpy.cumprod.html

Algorithm 1: The outer-loop part of the inverse design.

Input: The target haptic potential field, H^{target}, and the maximum number of magnets, n^{max}
Output: An optimal magnet arrangement (i.e., $\mathbf{x}^*$)
1 Perform pre-processing to H^{target};
2 Insert the first magnet (i.e., M_1) to the movable container;
3 **for** $i = 2, 3, \ldots, n^{max}$ **do**
4 Search for a good initial location and orientation to add a new magnet to the fixed container;
5 Insert a new magnet (i.e., M_i) to the found initial location and orientation;
6 Perform the inner-loop procedure (Algorithm 2) to adjust the arrangement of the magnets $\{M_1, \ldots, M_i\}$;
7 **if** *Termination condition is met* **then** break;
8 **end**
9 **return** The arrangement of the magnets $\{M_1, \ldots, M_i\}$;

- High-dimensional: the number of optimization variables is large.
- Global: there can be many local minima, most of which are not useful.
- Non-linear: both the objective and constraints are not simple linear functions.
- Non-differentiable: the derivatives of the objective and constraint functions are not available.

To our knowledge, no off-the-shelf solvers can handle this problem.

We propose the following three approximation techniques to solve the problem practically.

Approximation 1: Incrementally insert magnets one by one and stop this procedure when a termination condition is met, rather than simultaneously optimizing the arrangement of magnets and the number of magnets. This approximation resolves the issue of the optimization problem being trans-dimensional.

Approximation 2: Sequentially solve a small (low-dimensional) optimization problem for each magnet, rather than simultaneously solving a large (high-dimensional) optimization problem for all magnets. This approximation resolves the issue of the optimization problem being high-dimensional.

Approximation 3: Apply the *penalty method* [17] to reformulate the constrained optimization problem into a series of unconstrained optimization problems. This approximation allows the use of unconstrained optimization algorithms.

Taking these three techniques into consideration, we describe the overall optimization procedure as an "outer"-loop part, shown in Algorithm 1, and an "inner"-loop part, shown in Algorithm 2. The outer-loop part involves **Approximation 1**, and it iteratively calls the inner-loop part (line 6) in its loop. The inner-loop part involves **Approximations 2 and 3**, and it iteratively solves a much easier optimization problem (line 4), which is still non-linear and non-differentiable but can be handled by off-the-shelf solvers if we choose them appropriately.

In addition to these approximation techniques, we also propose a technique to estimate a reasonable initial solution when inserting

Algorithm 2: The inner-loop part of the inverse design.

```
  Input: The target haptic potential field, H^target, and the
         initial arrangement of the i magnets, {M_1, ..., M_i}
  Output: An optimal magnet arrangement of the i magnets
1 for j = 1, 2, ..., n^penalty do
2   | Solve the optimization problem to adjust the
    |   arrangement of the magnet M_i;
3   | for k = 1, 2, ..., i do
4   | | Solve the optimization problem to adjust the
    | |   arrangement of the magnet M_k;
5   | end
6   | Increase the penalty coefficient σ;
7 end
8 return The arrangement of the magnets {M_1, ..., M_i};
```

a new magnet (line 4), which helps find a good local optimum without sticking to undesirable local optima. This initial solution estimation allows the use of efficient local optimization algorithms instead of prohibitively heavy global optimization algorithms (such as *Bayesian optimization* [28]).

In the following subsections, we first describe more detailed formulations of the objective (Section 7.2) and constraints (Section 7.3) in Equation 1. We then describe details of the techniques and steps in Algorithms 1 and 2.

7.2 Objective Formulation: Distance Metric for Haptic Potential Fields

The objective of the optimization problem, Equation 1, is defined as the distance between the simulated haptic potential field and the user-specified haptic potential field. As the definition of the distance function d, we use the line integral of their distance at each position. That is, given two haptic potential fields, H_1 and H_2, defined along the trajectory C, the distance is calculated by

$$\begin{aligned} d(H_1, H_2) &= \int_C \|H_1(t) - H_2(t)\| \, ds = \int_0^1 \|H_1(t) - H_2(t)\| \, dt \\ &\approx \frac{1}{N+1} \sum_{i=0}^{N} \left\| H_1\left(\frac{i}{N}\right) - H_2\left(\frac{i}{N}\right) \right\|, \end{aligned} \tag{18}$$

where N is the number of samples to approximately calculate the line integral ($N = 20$ in our implementation).

7.3 Constraint Formulation: Validity of Magnet Arrangements

As we described in Section 4, we consider two constraints that should be satisfied:

- all magnets are inside of the containers, and
- all magnets are collision-free.

We introduce constraint functions, $c^{\text{container}} : \mathcal{X} \to \mathbb{R}$ and $c^{\text{collision}} : \mathcal{X} \to \mathbb{R}$, to mathematically model these two constraints. We design these functions such that they return negative values when the magnet arrangement satisfies the constraints, and they return positive values when the magnet arrangement violates the constraints. Using these functions, Equation 1 can be rewritten as

$$\begin{aligned} \mathbf{x}^* = \ & \mathop{\arg\min}_{\mathbf{x} \in \mathcal{X}} d(H(\mathbf{x}), H^{\text{target}}) \\ & \text{subject to} \begin{cases} c^{\text{container}}(\mathbf{x}) \leq 0 \\ c^{\text{collision}}(\mathbf{x}) \leq 0 \end{cases} . \end{aligned} \tag{19}$$

More specifically, when the magnet arrangement is collision-free (i.e., satisfying the constraint), $c^{\text{collision}}$ returns a negative value that represents the shortest distance among the magnets in the scene. When there are collisions (i.e., violating the constraint), $c^{\text{collision}}$ returns a positive value that represents the largest penetration depth among the collided magnets in the scene. We design $c^{\text{container}}$ similarly. Our implementation uses FCL [21] to calculate these function values.

7.4 Pre-Processing of User Input

Before starting to solve the optimization problem, we perform pre-processing to the user-specified haptic potential field H^{target}, as in line 1 in Algorithm 1. This is because the user input may include undesirable small noises due to mouse manipulation accuracy. Thus, we first apply the Savitzky–Golay filter[4] to H^{target}.

7.5 Incremental Insertion of Magnets and Termination Condition

At the beginning of the inverse design procedure, both the movable and fixed containers do not contain any magnets. After the pre-processing, we insert the first magnet (i.e., M_1) to the movable container (line 2 in Algorithm 1). Then, we begin to perform the outer-loop procedure. In each iteration, we insert a new magnet (i.e., M_i if it is the i-th magnet in the scene) to the fixed container (line 5 in Algorithm 1) and then perform the inner-loop procedure (line 6 in Algorithm 1) to adjust the arrangement of the so-far inserted magnets. We stop the outer-loop procedure when a termination condition is met (line 7 in Algorithm 1). For this condition, we simply set a threshold for the acceptable distance, $d^{\text{threshold}}$, and check whether the current distance between the simulated haptic potential field and the user-specified one is smaller than $d^{\text{threshold}}$, or not. If it is true, then the outer-loop part terminates and returns the solution obtained so far to the user (line 9 in Algorithm 1). Our implementation adaptively sets $d^{\text{threshold}}$ based on H^{target}; more specifically, the 5% of the value, $\max_t H^{\text{target}}(t) - \min_t H^{\text{target}}(t)$.

7.6 Estimation of Good Initial Solution

It is crucial to have a good initial solution in our problem setting since our problem is a global optimization with many useless local minima. To obtain a good initial arrangement of the first magnet, M_1, we perform the following procedure.

- Discretize the volumes of the movable and fixed containers using uniform grids.
- For each grid cell in the movable container, calculate the line integral of the distance to the closest grid cell in the fixed container along the trajectory.
- Choose the grid cell in the movable container that has the smallest value and call it G^{movable}.

[4] https://docs.scipy.org/doc/scipy/reference/generated/scipy.signal.savgol_filter.html

- Use the center of G^{movable} as the initial position.
- Use "N-up" (i.e., the N pole faces up) as the initial orientation.

To obtain a good initial arrangement of the i-th magnet, M_i ($i \geq 2$), we perform the following procedure.

- Find the parameter t that produces the maximum residual (i.e., the parameter t in which the difference between the target and current simulated haptic potential values become the largest) and call it t'.
- Move the movable container to $t = t'$.
- Choose the grid cell that is closest to G^{movable} from the fixed container.
- Use the center of the chosen grid cell as the initial position.
- Use either "N-up" or "S-up" (determined based on the sign of the residual) as the initial orientation.

7.7 Penalty Method

The penalty method [17] is one of the methods that solve a constrained optimization problem by decomposing it into a series of unconstrained optimization subproblems. It iteratively refines the solution by using the solution in the previous subproblem as the initial solution in the next subproblem. It adds *penalty* terms to the original objective, each of which represents how much the corresponding constraint is violated. That is, the value of the penalty term is zero if the constraint is satisfied, and the value becomes larger as the constraint gets violated. It increases the weight for the penalty term each time (line 6 in Algorithm 2), so that the final solution (mostly) satisfies the constraints. The j-th subproblem to solve Equation 19 is described as

$$\mathbf{x}^* = \mathop{\arg\min}_{\mathbf{x} \in \mathcal{X}} \left[\frac{1}{h} d(H(\mathbf{x}), H^{\text{target}}) + \sigma_j \left\{ g(c^{\text{container}}(\mathbf{x})) + w g(c^{\text{collision}}(\mathbf{x})) \right\} \right], \quad (20)$$

where $g(x) = \max(0, x)^2$, $h = \max_t H^{\text{target}}(t) - \min_t H^{\text{target}}(t)$, $\sigma_j \in \mathbb{R}_{>0}$ is the penalty weight at the j-th iteration of the penalty method, and w is a constant parameter for balancing the constraints (empirically set to 1.0×10^{-3}). Note that normalizing the distance by $\frac{1}{h}$ here is only optional but this can make the setting of the penalty weights less dependent on the user input H^{target}. Our implementation solves this subproblem twice (i.e., $n^{\text{penalty}} = 2$ in Algorithm 2) using $\sigma_1 = 5.0 \times 10^4$ and $\sigma_2 = 2.0 \times 10^5$ by default.

7.8 Magnet-by-Magnet Optimization

Each magnet has the degrees of freedom of a rigid body transformation, $SE(3)$. For this, we use the Cartesian coordinates representation (which is three-dimensional) to indicate the translational component and the rotation vector representation[5] (which is three-dimensional) to indicate the rotational component. Thus, the degrees of freedom of the k-th magnet, $\mathbf{x}_k$, is a 6-dimensional vector in our implementation. Note that the reason for using the rotation vector representation as optimization variables is that this representation is smooth and unbounded, is free from gimbal lock, and does not require normalization or orthogonalization (unlike the Euler angles, quaternion, and matrix representations).

As described in **Approximation 2** in Section 7.1, we solve Equation 20 for each magnet sequentially, not simultaneously. By this technique, we avoid directly solving the $6i$-dimensional optimization problem, where i is the number of magnets, and instead solve 6-dimensional optimization subproblems (see lines 3–5 in Algorithm 2). Now that each optimization problem is sufficiently tractable, we apply the Nelder–Mead method[6] available in SciPy [33], which is a popular choice for non-linear, non-differentiable, and reasonably local and low-dimensional optimization problems. Note that the reason for solving the 6-dimensional optimization problem for the new magnet first (line 2) is that the new magnet is likely to be in a relatively unreasonable configuration compared to other magnets, and thus it is effective to adjust its arrangement first.

8 TECHNICAL EVALUATION

Figure 3 shows the results of our inverse design procedure with various inputs, including haptic curves with linear slopes or multiple peaks, and trajectories with a straight or curved path. Even for these challenging inputs, our solver could successfully find reasonable and non-trivial magnet arrangements that well reproduce the target haptic curves. Refer to the video figure as well, which provides detailed visualizations of how our optimization procedure searched for the magnet arrangements for these cases. These results successfully validate that our proposed computational approach to magnetic force feedback design can be achieved by our proposed techniques.

We also conducted additional experiments to further validate the effectiveness of each technique. Our implementation runs on a MacBook Pro (Processor 2.6 GHz Quad-Core Intel Core i7 and Memory 16 GB). It is written with Python for optimization and C++ for magnetic simulation. The simulation part is accelerated by using OpenCL and runs on GPU (AMD Radeon Pro 450).

Effectiveness of Initial Solution Estimation. Our optimization solver has a heuristic initial solution estimation (Section 7.6) in its procedure. To validate the effectiveness of this estimation, we performed a custom optimization procedure that is identical to the proposed one except that it randomly initializes the newly added magnet's position. For this, we used the same input as Dial (1) in Figure 3. Figure 7 shows the result, in which the solver clearly failed to find a reasonable solution, and the reproduced haptic curve was quite different from the target one. This implies that our target optimization problem has many useless local minima, and our technique of initial solution estimation could reasonably resolve this issue.

Effectiveness of Magnet-by-Magnet Optimization. As discussed in Section 7.8, we avoid directly solving a $6n$-dimensional problem, where n is the number of magnets, but we solve 6-dimensional subproblems iteratively. To validate the effectiveness of this technique, we compared our optimization procedure with a custom one in which the sequential 6-dimensional subproblems were replaced with a single $6n$-dimensional problem. For this, we used the same input as the second example in Figure 3. As a result, we

[5] https://docs.scipy.org/doc/scipy/reference/generated/scipy.spatial.transform.Rotation.html

[6] https://docs.scipy.org/doc/scipy/reference/optimize.minimize-neldermead.html

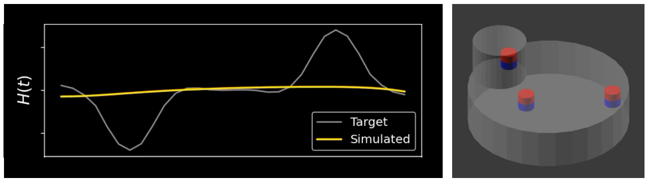

Figure 7: Result of using random initialization instead of using our initialization technique. It failed to find a reasonable solution.

observed that both the procedures could find reasonable solutions (more specifically, the magnet arrangements were different, but the reproduced haptic curves were mostly identical). However, the procedure that solved $6n$-dimensional problems took 35 minutes and 57 seconds to achieve convergence, while ours took only 3 minutes and 57 seconds.

Necessity of Penalty Method. We formulated the inverse design problem as a constrained optimization problem, and our solver handles the constraints by the penalty method (Section 7.7). To confirm the necessity of this technique, we performed an optimization procedure without adding the penalty of the constraints. For this, we used the same input as Dial (1) in Figure 3. Although the target haptic curve is well reproduced, two of the three magnets protrude from the containers.

9 DISCUSSION

Physical and Perceptual Validation. We did not perform measurement of magnetic forces (e.g., using a force gauge) for validation of magnetic simulation. This is because Yuang et al. [37] already performed a comparison test with analytical calculation and validated the simulation accuracy, and Thomaszewski et al. [30] also compared this approach [37] with the analytical approach [1]. As for the perception, Ogata [18] already validated the perceptual aspect of haptic potential field.

Physically Invalid Inputs. It is possible that the user-specified haptic potential field is physically invalid (i.e., not achievable by any magnet arrangements), such as the one with spikes or high-frequency waves. In such cases, the inverse design process cannot converge to a satisfactory solution that well reproduces the target. When this occurs, it is possible to warn the user that the target haptics could not be achieved well and needs to be fixed.

Non Quasi-Static Settings. Our method assumes a quasi-static setting as discussed in Section 5.1. This assumption is not valid when, for example, the user manipulates the movable container back and forth very quickly. In this case, the kinetic energy needs to be considered in addition to the potential energies. It is an important future work to model both the potential and kinetic energies as a unified haptic model.

Frictions. The haptic potential field can be understood as the work done by the finger in a frictionless environment (Section 5.8). This implies a limitation: our current formulation ignores the effect of frictions. We observed that the frictional force in our applications (Section 3.2) was not large compared to the magnetic force, and it did not qualitatively change the characteristics of the perceived haptic curves. Thus, this limitation is not critical, at least in our cases. Nonetheless, allowing users to design haptics in a friction-aware manner would be an important future work, making the design space broader. In terms of techniques, our theory (Section 5) is already capable of quantifying the contribution of friction to haptic feedback in a unified framework, and this goal can be achieved by integrating the work done against the frictional force (Equation 13) into the objective of the inverse design. Note that the frictional force could be simulated by putting additional assumptions on the friction model (e.g., Coulomb's friction law), the direction of the force applied by the fingers, and so on. Another challenge regarding this future work is the user specification; the input haptic curve may be less intuitive for users since it is no longer understood as a field (in a physics sense) with friction.

Gravity. Our current implementation focuses on the magnetic potential as the source of force feedback. However, the definition of the haptic potential field (Equation 8) allows us to design haptics by taking gravitational potential into consideration as well. If we handle trajectories that involve vertical movements, extending the implementation using the gravitational effect would be useful to model the perceived haptics more accurately.

Optimization Solver Accuracy. We demonstrated that our optimization solver could produce useful and non-trivial magnet arrangements for various inputs. Yet, since it relies on approximation techniques, it is possible that there exists a better solution than the one found by the solver. For example, our solver cannot guarantee that the number of used magnets is minimal.

Electromagnet. We focused on the use of permanent magnets (not electromagnets) since they need no power supply or electric wiring and thus are suitable for embedded haptics in everyday objects. Nonetheless, it is an interesting future work to investigate the use of electromagnets to render haptic potential fields. As electromagnets can be programmable, this would broaden the design space of interactions. Note that our discussions on haptic potential field (Section 5) is directly useful even in this advanced scenario.

10 CONCLUSION

We demonstrated that our approach could produce non-trivial designs to achieve desired magnetic force feedback, offering a new way to augment physical components for effective tangible interaction. As the magnetic force is an essential part of the source of any mechanical power, the combination with a computational approach with inverse design has various potentials. We envision a future world where we design our living environment with the power of computational design and physical simulation. With the current development of digital fabrication technology, we believe the combination of computational design and haptic design backed up by physics will open up new methodologies for interaction.

REFERENCES

[1] G. Akoun and J. . Yonnet. 1984. 3D analytical calculation of the forces exerted between two cuboidal magnets. *IEEE Transactions on Magnetics* 20, 5 (1984), 1962–1964. https://doi.org/10.1109/TMAG.1984.1063554

[2] Thomas Auzinger, Wolfgang Heidrich, and Bernd Bickel. 2018. Computational Design of Nanostructural Color for Additive Manufacturing. *ACM Trans. Graph.* 37, 4, Article 159 (July 2018), 16 pages. https://doi.org/10.1145/3197517.3201376

[3] Moritz Bächer, Emily Whiting, Bernd Bickel, and Olga Sorkine-Hornung. 2014. Spin-It: Optimizing Moment of Inertia for Spinnable Objects. *ACM Trans. Graph.* 33, 4, Article 96 (July 2014), 10 pages. https://doi.org/10.1145/2601097.2601157

[4] Bernd Bickel, Moritz Bächer, Miguel A. Otaduy, Hyunho Richard Lee, Hanspeter Pfister, Markus Gross, and Wojciech Matusik. 2010. Design and Fabrication of Materials with Desired Deformation Behavior. *ACM Trans. Graph.* 29, 4, Article 63 (July 2010), 10 pages. https://doi.org/10.1145/1778765.1778800

[5] John MD Coey. 2010. *Magnetism and magnetic materials.* Cambridge university press.

[6] Oskar Elek, Denis Sumin, Ran Zhang, Tim Weyrich, Karol Myszkowski, Bernd Bickel, Alexander Wilkie, and Jaroslav Křivánek. 2017. Scattering-Aware Texture Reproduction for 3D Printing. *ACM Trans. Graph.* 36, 6, Article 241 (Nov. 2017), 15 pages. https://doi.org/10.1145/3130800.3130890

[7] Eisuke Fujinawa, Shigeo Yoshida, Yuki Koyama, Takuji Narumi, Tomohiro Tanikawa, and Michitaka Hirose. 2017. Computational Design of Hand-Held VR Controllers Using Haptic Shape Illusion. In *Proceedings of the 23rd ACM Symposium on Virtual Reality Software and Technology* (Gothenburg, Sweden) *(VRST '17)*. Association for Computing Machinery, New York, NY, USA, Article 28, 10 pages. https://doi.org/10.1145/3139131.3139160

[8] Ruslan Guseinov, Eder Miguel, and Bernd Bickel. 2017. CurveUps: Shaping Objects from Flat Plates with Tension-Actuated Curvature. *ACM Trans. Graph.* 36, 4, Article 64 (July 2017), 12 pages. https://doi.org/10.1145/3072959.3073709

[9] Vincent Hayward. 2008. A brief taxonomy of tactile illusions and demonstrations that can be done in a hardware store. *Brain research bulletin* 75, 6 (2008), 742–752.

[10] Ralph Hollis. 2008. Maglev Haptics: Butterfly Haptic's New User Interface Technology. In *ACM SIGGRAPH 2008 New Tech Demos* (Los Angeles, California) *(SIGGRAPH '08)*. ACM, New York, NY, USA, Article 23, 1 pages. https://doi.org/10.1145/1401615.1401638

[11] Seung-Wook Kim, Sun Young Park, and Junghyun Han. 2018. Magnetization Dynamics for Magnetic Object Interactions. *ACM Trans. Graph.* 37, 4, Article 121 (July 2018), 13 pages. https://doi.org/10.1145/3197517.3201402

[12] Yuki Koyama and Masataka Goto. 2018. OptiMo: Optimization-Guided Motion Editing for Keyframe Character Animation. In *Proceedings of the 2018 CHI Conference on Human Factors in Computing Systems.* Association for Computing Machinery, New York, NY, USA, 1–12. https://doi.org/10.1145/3173574.3173735

[13] Thomas Langerak, Juan José Zárate, David Lindlbauer, Christian Holz, and Otmar Hilliges. 2020. Omni: Volumetric Sensing and Actuation of Passive Magnetic Tools for Dynamic Haptic Feedback. In *Proceedings of the 33rd Annual ACM Symposium on User Interface Software and Technology* (Virtual Event, USA) *(UIST '20)*. Association for Computing Machinery, New York, NY, USA, 594–606. https://doi.org/10.1145/3379337.3415589

[14] Karon E MacLean. 2008. Haptic interaction design for everyday interfaces. *Reviews of Human Factors and Ergonomics* 4, 1 (2008), 149–194.

[15] Luigi Malomo, Jesús Pérez, Emmanuel Iarussi, Nico Pietroni, Eder Miguel, Paolo Cignoni, and Bernd Bickel. 2018. FlexMaps: Computational Design of Flat Flexible Shells for Shaping 3D Objects. *ACM Trans. Graph.* 37, 6, Article 241 (Dec. 2018), 14 pages. https://doi.org/10.1145/3272127.3275076

[16] Xingyu Ni, Bo Zhu, Bin Wang, and Baoquan Chen. 2020. A Level-Set Method for Magnetic Substance Simulation. *ACM Trans. Graph.* 39, 4, Article 29 (July 2020), 15 pages. https://doi.org/10.1145/3386569.3392445

[17] Jorge Nocedal and Stephen J. Wright. 2006. *Numerical Optimization* (2nd ed.). Springer Science+Business Media. https://doi.org/10.1007/978-0-387-40065-5

[18] Masa Ogata. 2018. Magneto-Haptics: Embedding Magnetic Force Feedback for Physical Interactions. In *Proceedings of the 31st Annual ACM Symposium on User Interface Software and Technology* (Berlin, Germany) *(UIST '18)*. Association for Computing Machinery, New York, NY, USA, 737–743. https://doi.org/10.1145/3242587.3242615

[19] Masa Ogata and Masaaki Fukumoto. 2015. FluxPaper: Reinventing Paper with Dynamic Actuation Powered by Magnetic Flux. In *Proceedings of the 33rd Annual ACM Conference on Human Factors in Computing Systems* (Seoul, Republic of Korea) *(CHI '15)*. ACM, New York, NY, USA, 29–38. https://doi.org/10.1145/2702123.2702516

[20] Antti Oulasvirta, Niraj Ramesh Dayama, Morteza Shiripour, Maximilian John, and Andreas Karrenbauer. 2020. Combinatorial Optimization of Graphical User Interface Designs. *Proc. IEEE* 108, 3 (March 2020), 434–464. https://doi.org/10.1109/JPROC.2020.2969687

[21] Jia Pan, Sachin Chitta, and Dinesh Manocha. 2012. FCL: A General Purpose Library for Collision and Proximity Queries. In *2012 IEEE International Conference on Robotics and Automation.* 3859–3866. https://doi.org/10.1109/ICRA.2012.6225337

[22] Michal Piovarči, Danny M. Kaufman, David I. W. Levin, and Piotr Didyk. 2020. Fabrication-in-the-Loop Co-Optimization of Surfaces and Styli for Drawing Haptics. *ACM Trans. Graph.* 39, 4, Article 116 (July 2020), 16 pages. https://doi.org/10.1145/3386569.3392467

[23] Michal Piovarči, David I. W. Levin, Danny M. Kaufman, and Piotr Didyk. 2018. Perception-Aware Modeling and Fabrication of Digital Drawing Tools. *ACM Trans. Graph.* 37, 4, Article 123 (July 2018), 15 pages. https://doi.org/10.1145/3197517.3201322

[24] Michal Piovarči, David I. W. Levin, Jason Rebello, Desai Chen, Roman Ďurikovič, Hanspeter Pfister, Wojciech Matusik, and Piotr Didyk. 2016. An Interaction-Aware, Perceptual Model for Non-Linear Elastic Objects. *ACM Trans. Graph.* 35, 4, Article 55 (July 2016), 13 pages. https://doi.org/10.1145/2897824.2925885

[25] Romain Prévost, Emily Whiting, Sylvain Lefebvre, and Olga Sorkine-Hornung. 2013. Make It Stand: Balancing Shapes for 3D Fabrication. *ACM Trans. Graph.* 32, 4, Article 81 (July 2013), 10 pages. https://doi.org/10.1145/2461912.2461957

[26] Gabriel Robles-De-La-Torre and Vincent Hayward. 2001. Force can overcome object geometry in the perception of shape through active touch. *Nature* 412, 6845 (01 Jul 2001), 445–448. https://doi.org/10.1038/35086588

[27] Christian Schumacher, Bernd Bickel, Jan Rys, Steve Marschner, Chiara Daraio, and Markus Gross. 2015. Microstructures to Control Elasticity in 3D Printing. *ACM Trans. Graph.* 34, 4, Article 136 (July 2015), 13 pages. https://doi.org/10.1145/2766926

[28] Bobak Shahriari, Kevin Swersky, Ziyu Wang, Ryan P. Adams, and Nando de Freitas. 2016. Taking the Human Out of the Loop: A Review of Bayesian Optimization. *Proc. IEEE* 104, 1 (January 2016), 148–175. https://doi.org/10.1109/JPROC.2015.2494218

[29] Mélina Skouras, Bernhard Thomaszewski, Stelian Coros, Bernd Bickel, and Markus Gross. 2013. Computational Design of Actuated Deformable Characters. *ACM Trans. Graph.* 32, 4, Article 82 (July 2013), 10 pages. https://doi.org/10.1145/2461912.2461979

[30] Bernhard Thomaszewski, Andreas Gumann, Simon Pabst, and Wolfgang Straßer. 2008. Magnets in Motion. *ACM Trans. Graph.* 27, 5, Article 162 (Dec. 2008), 9 pages. https://doi.org/10.1145/1409060.1409115

[31] Chelsea Tymms, Esther P. Gardner, and Denis Zorin. 2018. A Quantitative Perceptual Model for Tactile Roughness. *ACM Trans. Graph.* 37, 5, Article 168 (Oct. 2018), 14 pages. https://doi.org/10.1145/3186267

[32] Nobuyuki Umetani, Yuki Koyama, Ryan Schmidt, and Takeo Igarashi. 2014. Pteromys: Interactive Design and Optimization of Free-Formed Free-Flight Model Airplanes. *ACM Trans. Graph.* 33, 4, Article 65 (July 2014), 10 pages. https://doi.org/10.1145/2601097.2601129

[33] Pauli Virtanen, Ralf Gommers, Travis E. Oliphant, Matt Haberland, Tyler Reddy, David Cournapeau, Evgeni Burovski, Pearu Peterson, Warren Weckesser, Jonathan Bright, Stéfan J. van der Walt, Matthew Brett, Joshua Wilson, K. Jarrod Millman, Nikolay Mayorov, Andrew R. J. Nelson, Eric Jones, Robert Kern, Eric Larson, CJ Carey, İlhan Polat, Yu Feng, Eric W. Moore, Jake Vand erPlas, Denis Laxalde, Josef Perktold, Robert Cimrman, Ian Henriksen, E. A. Quintero, Charles R Harris, Anne M. Archibald, Antônio H. Ribeiro, Fabian Pedregosa, Paul van Mulbregt, and SciPy 1.0 Contributors. 2020. SciPy 1.0: Fundamental Algorithms for Scientific Computing in Python. *Nature Methods* 17 (2020), 261–272. https://doi.org/10.1038/s41592-019-0686-2

[34] Malte Weiss, Chat Wacharamanotham, Simon Voelker, and Jan Borchers. 2011. FingerFlux: Near-surface Haptic Feedback on Tabletops. In *Proceedings of the 24th Annual ACM Symposium on User Interface Software and Technology* (Santa Barbara, California, USA) *(UIST '11)*. ACM, New York, NY, USA, 615–620. https://doi.org/10.1145/2047196.2047277

[35] Kentaro Yasu. 2017. Magnetic Plotter: A Macrotexture Design Method Using Magnetic Rubber Sheets. In *Proceedings of the 2017 CHI Conference on Human Factors in Computing Systems* (Denver, Colorado, USA) *(CHI '17)*. Association for Computing Machinery, New York, NY, USA, 4983–4993. https://doi.org/10.1145/3025453.3025702

[36] Kentaro Yasu. 2020. MagneLayer: Force Field Fabrication by Layered Magnetic Sheets. In *Proceedings of the 2020 CHI Conference on Human Factors in Computing Systems* (Honolulu, HI, USA) *(CHI '20)*. Association for Computing Machinery, New York, NY, USA, 1–9. https://doi.org/10.1145/3313831.3376552

[37] Kar W Yung, Peter B Landecker, and Daniel D Villani. 1998. An analytic solution for the force between two magnetic dipoles. *Physical Separation in Science and Engineering* 9, 1 (1998), 39–52.

[38] Jonas Zehnder, Espen Knoop, Moritz Bächer, and Bernhard Thomaszewski. 2017. Metasilicone: Design and Fabrication of Composite Silicone with Desired Mechanical Properties. *ACM Trans. Graph.* 36, 6, Article 240 (Nov. 2017), 13 pages. https://doi.org/10.1145/3130800.3130881

[39] Clement Zheng and Ellen Yi-Luen Do. 2018. Mechamagnets: Tactile Mechanisms with Embedded Magnets. In *Proceedings of the Twelfth International Conference on Tangible, Embedded, and Embodied Interaction* (Stockholm, Sweden) *(TEI '18)*. ACM, New York, NY, USA, 57–64. https://doi.org/10.1145/3173225.3173268